Pressure-induced enhancement of polar distortions in a metal and implications for the Rashba spin splitting

Evie Ladbrook,[1] Urmimala Dey,[2,3] Nicholas C. Bristowe,[2] Robin S. Perry,[4]
Dominik Daisenberger,[5] Mark R. Warren,[5] and Mark S. Senn[1,*]
[1]*Department of Chemistry, University of Warwick, Gibbet Hill, Coventry CV4 7AL, United Kingdom*
[2]*Centre for Materials Physics, Durham University, South Road, Durham DH1 3LE, United Kingdom*
[3]*Luxembourg Institute of Science and Technology (LIST), Avenue des Hauts-Fourneaux 5, L-4362 Esch-sur-Alzette, Luxembourg*
[4]*London Centre for Nanotechnology and Department of Physics and Astronomy, University College London,*
London WC1E 6BT, United Kingdom
[5]*Diamond Light Source Limited, Harwell Science and Innovation Campus, Didcot OX11 0DE, United Kingdom*

(Received 4 February 2025; revised 13 March 2025; accepted 24 April 2025; published 7 May 2025)

Polar metals are an intriguing class of materials that feature a polar crystal structure while also exhibiting metallic conductivity. The unique properties of polar metals challenge expectations, making way for the exploration of exotic phenomena such as unconventional magnetism, hyperferroelectric multiferroicity, and the development of multifunctional devices that can leverage both the material's polar structure and its asymmetry in the spin conductivity, that arises due to the Rashba effect. Here, via a high-pressure single-crystal diffraction study, we report the pressure-induced enhancement of polar distortions in such a metal, $Ca_3Ru_2O_7$. Our density functional theory calculations highlight that naive assumptions about the linear dependency between polar distortion amplitudes and the magnitude of the Rashba spin splitting may not be generally valid.

DOI: 10.1103/PhysRevB.111.205110

I. INTRODUCTION

Polar metals are an intriguing class of materials that feature a polar crystal structure while also exhibiting metallic conductivity. The concept of a ferroelectriclike transition in a metal was first predicted in 1965 [1] but not experimentally realized until such a transition was identified in metallic $LiOsO_3$ [2]. Several polar metals have been identified since then [3–5], with ferroelectric switching first being demonstrated in WTe_2 [6,7], defying assumptions that ferroelectricity and metallicity are mutually exclusive. The unique properties of polar metals do not only challenge expectations, making way for the exploration of exotic phenomena such as unconventional magnetism [8], hyperferroelectric multiferroicity [9], and unique topologies [10], but also open up the possibility for developing multifunctional devices [4,11–13].

The absence of an inversion center in combination with the spin-orbit interaction can facilitate the Rashba interaction. As polar metals can satisfy both requirements, they provide an obvious platform to explore this effect. Although the Rashba interaction has most commonly been studied at surfaces and interfaces [14,15], where inversion symmetry is necessarily broken, the effect has also been demonstrated in bulk systems [16–18]. This has implications to the field of spintronics [19], where electron spins, rather than just the charge, may be manipulated by an electric field.

In many polar metals, the polar mode arises through a "geometric mechanism" as conventional chemical mechanisms for ferroelectricity are broadly incompatible with metallicity [3,4,20,21]. Typically, free electrons would screen the long-range interactions responsible for ferroelectricity, inhibiting the formation of a permanent electric dipole. However, materials in which a polar mode arises due to a structural instability may circumvent this. One mechanism is via a "hybrid improper" mechanism [22], prototypical to $n = 2$ Ruddlesden-Popper (RP) phase $Ca_3Mn_2O_7$, where polarization arises due to the trilinear coupling between two nonpolar structural distortions, the tilting and rotation of the MnO_6 octahedra in the case of $Ca_3Mn_2O_7$, with a polar distortion mode, as shown in Fig. 1.

$Ca_3Ru_2O_7$ is a member of the $n = 2$ RP family, crystallizing in the polar $Bb2_1m$ space group (nonstandard setting of $Cmc2_1$), however, it has a metallic ground state [23,24]. Although ferroelectric switching cannot be achieved by application of an external electric field, a recent study has revealed a polar domain structure consisting of 90° and 180° domain walls with ferroelastic domains that can be switched by applied uniaxial strain [24]. $Ca_3Ru_2O_7$ also undergoes a spin reorientation transition where, upon cooling from 60 to 48 K, the spins reorient from aligning along the crystallographic a axis, aligning ferromagnetically within each perovskite layer and antiferromagnetically between them, to be parallel to b

---

[*] Contact author: m.senn@warwick.ac.uk

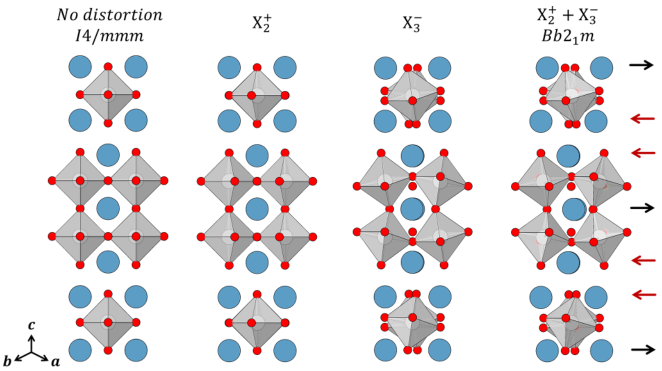

FIG. 1. An $n = 2$ Ruddlesden-Popper structure consisting of two perovskite layers separated by a rocksaltlike layer with representation of the distortion of the theoretical high-symmetry $I4/mmm$ to the orthorhombic $Bb2_1m$ phase through octahedral rotations (X_2^+) and tilts (X_3^-). Arrows indicate the polar distortions, primarily consisting of Ca displacements.

[23,25,26]. The coupling between the spin ordering direction and the polar crystallographic axis via a strong spin-orbit interaction induces the Rashba-like spin splitting in momentum space [27]. Very recently, it has been shown that this transition can be induced by application of uniaxial strain which emphasizes how the structural, magnetic, and electronic degrees of freedom are intricately coupled [28].

Similarly, pressure can be used to directly probe the interplay between the structural, octahedral rotations, and tilts [29], and polar distortions with a view to understanding how the Rashba spin splitting might be tuned in polar metals. Although it is generally understood that the initial application of hydrostatic pressure suppresses the polar distortion in conventional proper ferroelectrics, such as $BaTiO_3$ [30,31], as they tend to undergo a phase transition to a nonpolar state, this does not necessarily hold true for all ferroelectrics. For example, in the case of the hybrid improper mechanism, we have recently shown, by powder x-ray diffraction in combination with density functional theory calculations (DFT), that the polar distortion can be enhanced in the insulator $Ca_3Ti_2O_7$ by pressure [32].

The prospect of coupling spin transport properties to external stimuli such as pressure via internal structural degrees of freedom, such as octahedral rotations, and their coupling to polar modes, is intriguing. Naively, we might assume that the amplitude of the Rashba effect has a linear dependence on the polar mode, as shown for surfaces, interfaces, and bulk systems [33–37], however, there are indications in the literature that this situation may be somewhat more complex [38].

Here, we report the results of our high-pressure single-crystal diffraction studies on $Ca_3Ru_2O_7$ that show that the structural ingredients, necessary for enhancing the amplitude of the polar mode in a metal, are systematically enhanced up to 15 GPa. Our first-principles calculations within density functional theory (DFT) reveal that, contrary to expectations, the enhancement of the polar mode manifests itself in a decrease in spin splitting in momentum space.

II. EXPERIMENTAL DETAILS

Single-crystal samples were selected from the same growth batch as those which demonstrated incommensurate magnetism at 50 K [39]. All samples were confirmed as single phase and good quality via magnetization, resistivity, and scanning electron microscopy/energy-dispersive x-ray spectroscopy (SEM/EDX) measurements.

A single crystal of dimensions $50 \times 30 \times 15$ μm was loaded into a Le Toullec diamond anvil cell (DAC) equipped with Boehler-Almax anvils with 400-μm culets and a rhenium gasket which was preindented to 50 μm with a 250-μm-diameter sample chamber eroded into the indent. Helium was used as a pressure transmitting medium to ensure the sample was compressed under hydrostatic pressure. A ruby sphere was used as a pressure indicator [40]. Single-crystal x-ray diffraction measurements were performed using a four-axis Newport diffractometer equipped with a Dectris Eiger CdTe detector, operating at a wavelength of $\lambda = 0.4859$ Å (corresponding to a beam energy of approximately 25.5 keV), in Experimental Hutch 2 (EH2) at Beamline I19 of the Diamond Light Source.

Indexing, integration, and refinalization were performed using CRYSALISPRO with a spherical absorption correction. The structure was initially solved for the ambient pressure collection using SHELXT [41] and subsequent pressures by isomorphous replacement, and then refined to convergence using SHELXL [42] implemented through OLEX2 [43]. The presence of inversion twinning was accounted for via the ([−1 0 0], [0 −1 0], [0 0 1]) twin law for which the batch scale factor (BASF) was fixed to 0.50.

III. HIGH-PRESSURE X-RAY DIFFRACTION RESULTS

High-pressure single-crystal x-ray diffraction data were collected between 0 and 14.5(2) GPa. Figure 2 shows how the experimentally refined lattice parameters and volume evolve with pressure compared to those calculated from DFT. Full computational details can be found in the Supplemental Material (SM) [44]. In both cases, the lattice parameters and volume decrease smoothly with pressure. Experimentally, we find that the compressibility of the *c* axis is smaller than that of the *a* and *b* axes. Additionally, the compressibility of *c* is slightly greater and *a* is smaller compared to that calculated by DFT. There is a more significant difference in the compressibility of *b*, which, as we show later, is linked to a small proper contribution to the polar mode instability in our DFT calculations. However, all of these discrepancies could arise as the DFT calculations were performed at 0 K while experimental measurements were carried out at room temperature. Compressibility parameters and Birch-Murnaghan coefficients were calculated using PASCAL [45] and are tabulated in the Supplemental Material (Tables S2 and S3 [44]).

To explore the evolution of the atomic level structure, the experimental and DFT-relaxed structures were then decomposed in terms of symmetry-adapted displacements using ISODISTORT [46,47]. The $Bb2_1m$ phase is related to the theoretical $I4/mmm$ aristotype by an in-phase rotation and an out-of-phase tilt of the TiO_6 octahedra which transform as irreducible representations X_2^+ and X_3^-, respectively.

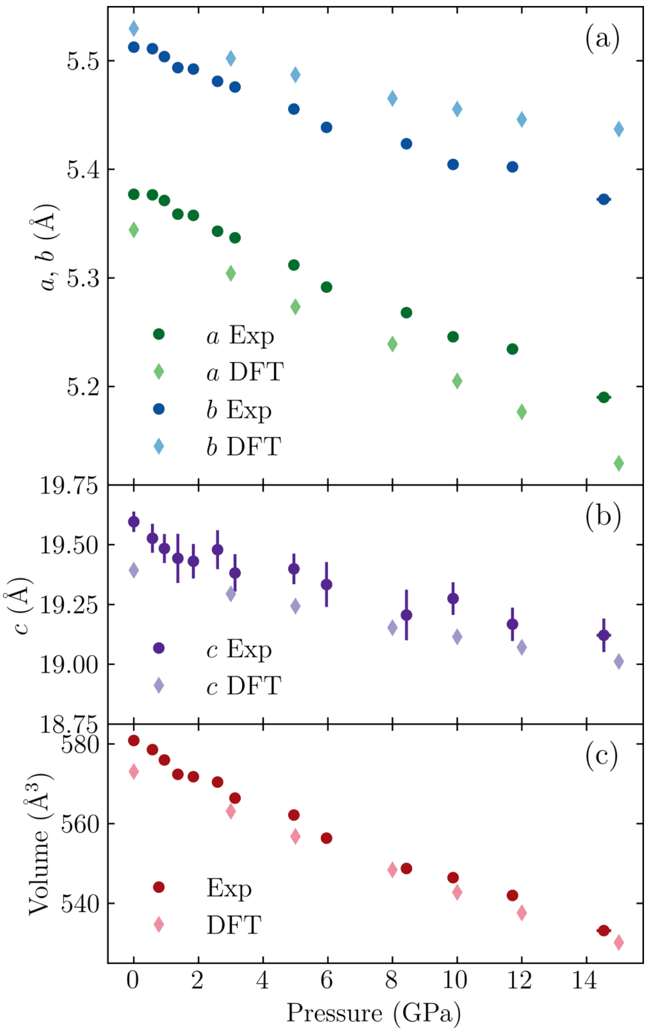

FIG. 2. (a) a, b and (b) c lattice parameters, and (c) unit cell volume extracted from variable-pressure single-crystal diffraction data and DFT calculations.

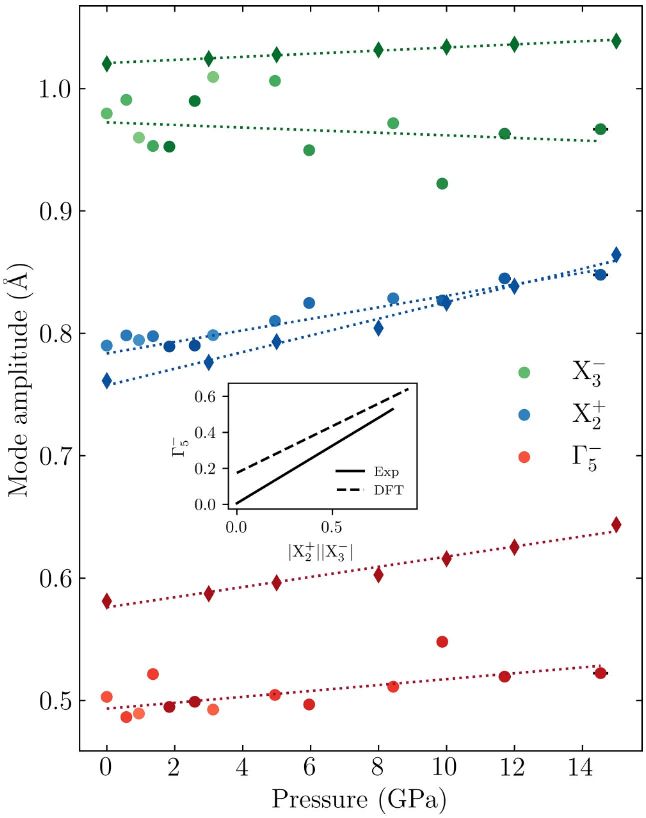

FIG. 3. Distortion mode amplitudes as a function of pressure for experimental (circles) and DFT calculated (diamonds) results. For the experimental results, a weighted linear regression was performed based on the R_1 statistics of the refined structures, with darker colors indicating a lower R_1 value. Refinement statistics are tabulated in the Supplemental Material (Table S1). The inset shows a plot of the product of the amplitude of the rotation (X_2^+) and tilt (X_3^-) modes, from these fits, against the polar mode (Γ_5^-) amplitude.

These couple to the polar displacement, which transforms as irreducible representation Γ_5^-, via the trilinear coupling mechanism. The resulting pressure-dependent symmetry distortion mode amplitudes are shown in Fig. 3.

The experimentally determined mode amplitudes show an overall steady increase in the amplitude of the rotation, X_2^+, while the amplitude of the tilt, X_3^-, remains relatively constant as the pressure increases. This aligns with the trends observed in compressibility, where a greater change in the a and b axes is associated with a larger change in the amplitude of rotation within the ab plane. Similarly, the smaller change in the c axis can be associated more to the stability of the tilt across the pressure range. Generally, extracting symmetry mode amplitudes from single-crystal data at high pressures is challenging due to restrictions concerning the experimental setup, such as the narrow opening angle of the DACs, meaning subtle structural changes become harder to resolve reliably as the pressure increases. However, despite some fluctuations in the experimentally determined mode amplitudes, these results show a good level of agreement with the DFT calculated mode amplitudes.

In accordance with the trilinear coupling mechanism, the amplitude of the polar distortion, Γ_5^-, should be linearly proportional to the product of the amplitudes of the driving order parameters, X_2^+ and X_3^- [22]. Since the individual values associated with the driving order parameters have some scatter, in the inset of Fig. 3, we instead show the relationship between the weighted linear regression fits to these order parameters. This illustrates that a zero intercept would be predicted on extrapolation. This confirms that, for the experimental data, the polar distortion is driven solely by the hybrid improper mechanism. However, for the DFT calculated results, the Γ_5^- amplitude is in excess of that expected by the trilinear mechanism. This suggests that there is a small proper contribution to the polar distortion, which, as shown in Fig. S3 [44], vanishes as the pressure increases above 10 GPa. This could be for a variety of reasons such as the difference in volume of the DFT unit cell, dependence on the pseudopotentials or exchange correlation functional, or it could be a real discrepancy between 0 K DFT and our room-temperature diffraction experiments. This also helps to clarify the discrepancy between the experimental and DFT calculated compressibility along b, as this is the polar axis. However, in general, the level

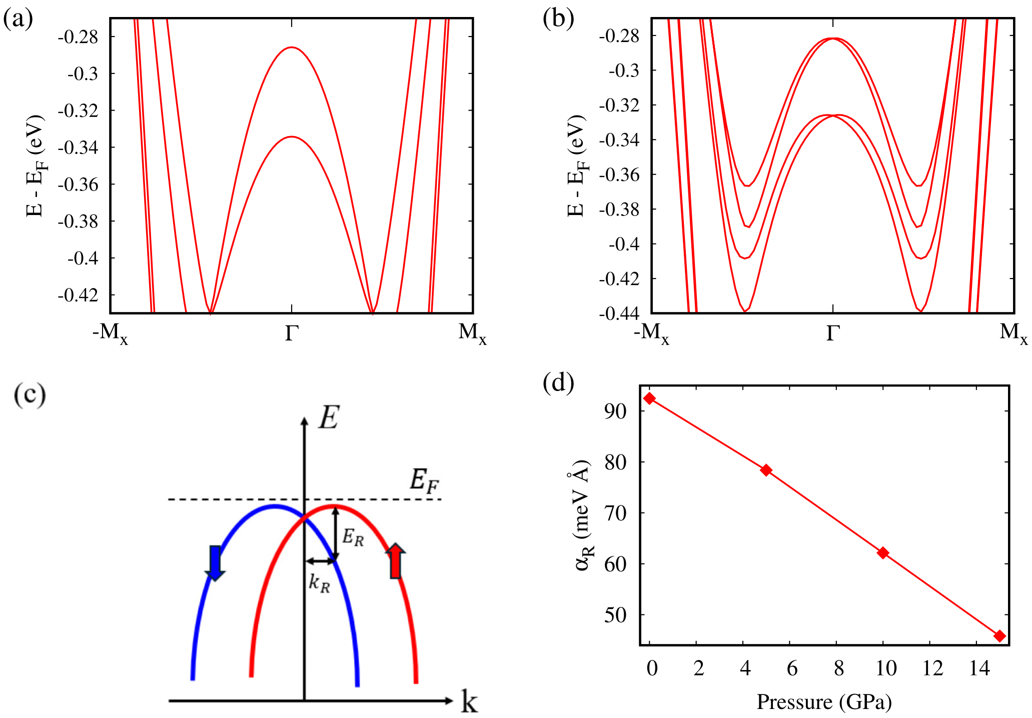

FIG. 4. Electronic band structure calculated at ambient pressure (a) without and (b) with SOC. E_F is the Fermi energy. (c) Schematic diagram illustrating the definition of Rashba parameter, where k_R is the distance between the crossing point of the Rashba spin-split bands and VBM, and E_R is the corresponding energy difference. Red and blue arrows indicate the up- and down-spin character of the bands, respectively. (d) Evolution of the Rashba parameter α_R in $Ca_3Ru_2O_7$ as a function of pressure.

of agreement, especially considering both the complexity of the electronic structure of these materials and the challenges of performing high-resolution x-ray diffraction at these pressures, is very good. The key point from both the experimental and DFT work is that that octahedral rotations are enhanced at a greater rate than the octahedral tilts are suppressed, resulting in an increase in the polar distortion via the trilinear mechanism. While this pressure-induced enhancement would be unexpected for a proper ferroelectric, we have recently predicted, via DFT calculations, a similar effect in insulating hybrid improper ferroelectric $Ca_3Ti_2O_7$ [32], and thus our experimental and DFT results are suggestive that this phenomena may be much more widespread.

IV. IMPLICATIONS TO RASHBA SPIN-SPLITTING

Motivated by our ability to enhance the polar distortion in this material as a function of pressure, we now turn our attention to the effect such enhancements might have on the band structure of these materials.

Figures 4(a) and 4(b) present the band structures calculated for the ambient-pressure $Bb2_1m$ structure of $Ca_3Ru_2O_7$ along the $-M_x$–Γ–M_x direction with and without spin-orbit coupling (SOC). We observe a sizable Rashba splitting of the bands around the Γ point near the valence band maximum (VBM) when SOC is turned on. Partial density of states calculations in Fig. S7 [44] reveal that the band splitting region is mostly contributed by Ru-d_{t2g} and O-p states.

To quantify the magnitude of the momentum-dependent Rashba splitting, we compute the Rashba parameter defined as $\alpha_R = 2E_R/k_R$, where k_R is the distance between the crossing point of the Rashba-split bands and VBM, and E_R is the corresponding energy splitting [33,34], as shown in Fig. 4(c). Surprisingly, the Rashba parameter calculated for the fully relaxed structures at different pressures reveals a monotonic decrease in α_R with increasing pressure [Fig. 4(d)]. Since the polar mode amplitude in $Ca_3Ru_2O_7$ increases with pressure (Fig. 3), this observation contradicts the conventional expectation that the Rashba parameter should scale with the polar mode amplitude [33–37]. In fact, the increase in the amplitude of the polar mode appears to be the primary cause of the reduction in the Rashba parameter.

To understand the decrease in the Rashba splitting with pressure, depicted in Fig. S6 [44], we compute the ambient-pressure band structure by setting the displacive components of the Ca, Ru, and O sites that transform as Γ_5^- to zero, as shown in Fig. 5. Note that even in the absence of the polar mode, the two tilt modes collectively polarize the electron clouds, leading to inversion symmetry breaking and thus preserving the $Bb2_1m$ structure. We find that the absence of the polar mode leads to a substantial enhancement of the Rashba parameter to ~172 meV Å, which is approximately 1.8 times greater than its value in the relaxed $Bb2_1m$ structure containing the polar mode as well as the two tilt modes (at zero pressure). Here, all other structural degrees of freedom, including unit cell parameters and hence volume are maintained at the values of the relaxed structure in which the polar distortions were present. Since all other structural modes, aside from the polar distortions, are equivalent for the band structures shown in Figs. 4(b) and 5, this appears

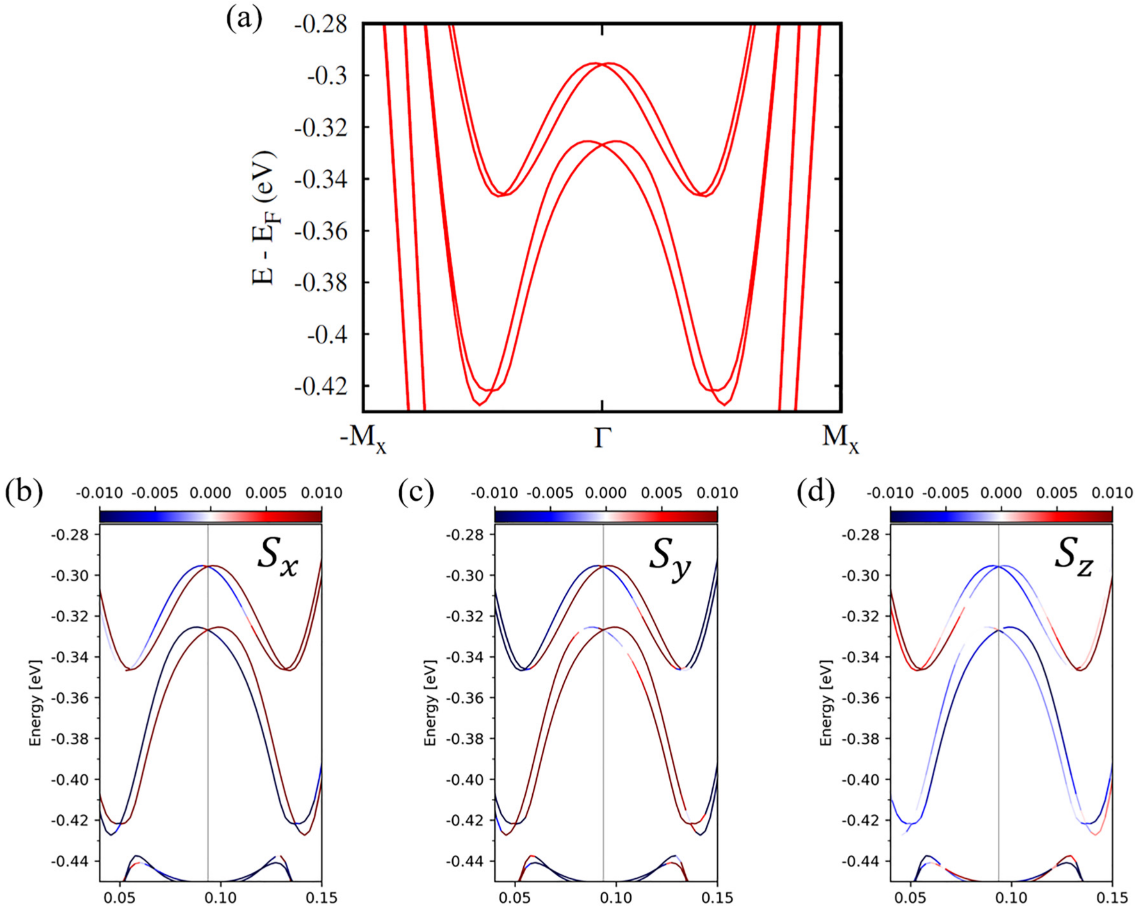

FIG. 5. (a) Band structure at ambient pressure calculated by setting the polar mode amplitude to zero (tilts only). (b)–(d) Corresponding spin-resolved band structures confirming the pure Rashba character of the bands at the VBM. SOC is included in these calculations.

to be indicative that the increasing polar mode amplitude as a function of pressure is predominantly responsible for the reduction in the Rashba spin splitting observed in Fig. 4(d). Additionally, the spin-projected band structures in Figs. 5(b)–5(d) reveal the splitting between spin-up and spin-down bands for the *x*- and *y*-spin components, confirming the pure Rashba character of the bands at the VBM [48].

Unpicking the multiple complexities of the pressure-dependent structure, and band structure, represents substantial further work. For example, we find that isovalent substitution of Ca for Hg in the isostructural $Bb2_1m$ phase results in a negligible change in the Rashba splitting with and without the polar mode. On the other hand, substitution of Ca for Cd leads to a drastic change in the band structure, reducing the magnitude of the Rashba spin splitting in the absence of the polar mode, despite a very small contribution from the *A*-site cations near the Fermi level in all cases. Our results are, therefore, strongly suggestive that the magnitude of the structural polar distortion is an insufficient proxy for the *k*-space spin-polarization dependence in this class of polar metals.

In conclusion, we have performed a detailed high-pressure investigation into the pressure dependence of the hybrid improper ordering parameters in polar metal, $Ca_3Ru_2O_7$. Our results show that, contrary to the situation predominantly observed for proper ferroelectrics, hydrostatic pressure actually acts to enhance the polar distortions in this materials. This comes about due to the increase in the magnitude of RuO_6 octahedral rotations, which form one of the primary order parameters of the hybrid improper mechanism. Curiously, despite the enhanced magnitude of the polar mode at high pressures, our theoretical calculations show that, counterintuitively, this would lead to a decrease in the Rashba spin splitting. Thus, our results highlight the Rashba effect in polar metals as a distinctive phenomenon worthy of further investigation.

ACKNOWLEDGMENTS

E.L. is thankful for support from the University of Warwick as a Ph.D. student through the Warwick Centre for Doctoral Training in Analytical Science and thanks M. Edwards for assistance in the collection of high-pressure x-ray diffraction data. U.D. and N.C.B. acknowledge the Leverhulme Trust for a research project grant (Grant No. RPG-2020-206). This work used the ARCHER2 UK National Supercomputing Service [49,50] and the Hamilton HPC Service of Durham University. M.S.S. acknowledges support as a Royal Society fellow (UF160265 and URF\R\231012) and EPSRC grant Novel Multiferroic Perovskites through Systematic Design (EP/S027106/1) for funding. The initial high-pressure diffraction studies were performed via the the Warwick x-ray Research Technology Platform. We acknowledge Diamond Light Source for time on Beamline I19 under Proposal No. CY36775-1.

DATA AVAILABILITY

The experimental data underpinning this study is available in the electronic supplemental materials.

---

[1] P. W. Anderson and E. I. Blount, Symmetry considerations on martensitic transformations: "Ferroelectric" metals? Phys. Rev. Lett. **14**, 217 (1965).

[2] Y. Shi, Y. Guo, X. Wang, A. J. Princep, D. Khalyavin, P. Manuel, Y. Michiue, A. Sato, K. Tsuda, S. Yu, M. Arai, Y. Shirako, M. Akaogi, N. Wang, K. Yamaura, and A. T. Boothroyd, A ferroelectric-like structural transition in a metal, Nat. Mater. **12**, 1024 (2013).

[3] T. H. Kim, D. Puggioni, Y. Yuan, L. Xie, H. Zhou, N. Campbell, P. J. Ryan, Y. Choi, J.-W. Kim, J. R. Patzner, S. Ryu, J. P. Podkaminer, J. Irwin, Y. Ma, C. J. Fennie, M. S. Rzchowski, X. Q. Pan, V. Gopalan, J. M. Rondinelli, and C. B. Eom, Polar metals by geometric design, Nature (London) **533**, 68 (2016).

[4] D. Puggioni and J. M. Rondinelli, Designing a robustly metallic noncenstrosymmetric ruthenate oxide with large thermopower anisotropy, Nat. Commun. **5**, 3432 (2014).

[5] T. Kolodiazhnyi, Insulator-metal transition and anomalous sign reversal of the dominant charge carriers in perovskite $BaTiO_{3-\delta}$, Phys. Rev. B **78**, 045107 (2008).

[6] Z. Fei, W. Zhao, T. A. Palomaki, B. Sun, M. K. Miller, Z. Zhao, J. Yan, X. Xu, and D. H. Cobden, Ferroelectric switching of a two-dimensional metal, Nature (London) **560**, 336 (2018).

[7] P. Sharma, F.-X. Xiang, D.-F. Shao, D. Zhang, E. Y. Tsymbal, A. R. Hamilton, and J. Seidel, A room-temperature ferroelectric semimetal, Sci. Adv. **5**, eaax5080 (2019).

[8] S. Lei, S. Chikara, D. Puggioni, J. Peng, M. Zhu, M. Gu, W. Zhao, Y. Wang, Y. Yuan, H. Akamatsu, M. H. W. Chan, X. Ke, Z. Mao, J. M. Rondinelli, M. Jaime, J. Singleton, F. Weickert, V. S. Zapf, and V. Gopalan, Comprehensive magnetic phase diagrams of the polar metal $Ca_3(Ru_{0.95}Fe_{0.05})_2O_7$, Phys. Rev. B **99**, 224411 (2019).

[9] W. Luo, K. Xu, and H. Xiang, Two-dimensional hyperferroelectric metals: A different route to ferromagnetic-ferroelectric multiferroics, Phys. Rev. B **96**, 235415 (2017).

[10] S.-Y. Xu, I. Belopolski, N. Alidoust, M. Neupane, G. Bian, C. Zhang, R. Sankar, G. Chang, Z. Yuan, C.-C. Lee, S.-M. Huang, H. Zheng, J. Ma, D. S. Sanchez, B. Wang, A. Bansil, F. Chou, P. P. Shibayev, H. Lin, S. Jia *et al.*, Discovery of a Weyl fermion semimetal and topological Fermi arcs, Science **349**, 613 (2015).

[11] D. Puggioni, G. Giovannetti, M. Capone, and J. M. Rondinelli, Design of a Mott multiferroic from a nonmagnetic polar metal, Phys. Rev. Lett. **115**, 087202 (2015).

[12] Q.-F. Yao, J. Cai, W.-Y. Tong, S.-J. Gong, J.-Q. Wang, X. Wan, C.-G. Duan, and J. H. Chu, Manipulation of the large Rashba spin splitting in polar two-dimensional transition-metal dichalcogenides, Phys. Rev. B **95**, 165401 (2017).

[13] X. Liu, Y. Yang, T. Hu, G. Zhao, C. Chen, and W. Ren, Vertical ferroelectric switching by in-plane sliding of two-dimensional bilayer WTe_2, Nanoscale **11**, 18575 (2019).

[14] K. V. Shanavas and S. Satpathy, Electric field tuning of the Rashba effect in the polar perovskite structures, Phys. Rev. Lett. **112**, 086802 (2014).

[15] S. Bhowal and S. Satpathy, Electric field tuning of the anomalous Hall effect at oxide interfaces, npj Comput. Mater. **5**, 61 (2019).

[16] D. Di Sante, P. Barone, R. Bertacco, and S. Picozzi, Electric control of the giant Rashba effect in bulk GeTe, Adv. Mater. **25**, 509 (2013).

[17] K. Ishizaka, M. S. Bahramy, H. Murakawa, M. Sakano, T. Shimojima, T. Sonobe, K. Koizumi, S. Shin, H. Miyahara, A. Kimura, K. Miyamoto, T. Okuda, H. Namatame, M. Taniguchi, R. Arita, N. Nagaosa, K. Kobayashi, Y. Murakami, R. Kumai, Y. Kaneko *et al.*, Giant Rashba-type spin splitting in bulk BiTeI, Nat. Mater. **10**, 521 (2011).

[18] K. Yamauchi, P. Barone, and S. Picozzi, Bulk Rashba effect in multiferroics: A theoretical prediction for $BiCoO_3$, Phys. Rev. B **100**, 245115 (2019).

[19] A. Manchon, H. C. Koo, J. Nitta, S. M. Frolov, and R. A. Duine, New perspectives for Rashba spin–orbit coupling, Nat. Mater. **14**, 871 (2015).

[20] S. Bhowal and N. A. Spaldin, Polar metals: Principles and prospects, Annu. Rev. Mater. Res. **53**, 53 (2023).

[21] N. A. Benedek and T. Birol, Ferroelectric metals reexamined: Fundamental mechanisms and design considerations for new materials, J. Mater. Chem. C **4**, 4000 (2016).

[22] N. A. Benedek and C. J. Fennie, Hybrid improper ferroelectricity: A mechanism for controllable polarization-magnetization coupling, Phys. Rev. Lett. **106**, 107204 (2011).

[23] G. Cao, S. McCall, J. E. Crow, and R. P. Guertin, Observation of a metallic antiferromagnetic phase and metal to nonmetal transition in $Ca_3Ru_2O_7$, Phys. Rev. Lett. **78**, 1751 (1997).

[24] S. Lei, M. Gu, D. Puggioni, G. Stone, J. Peng, J. Ge, Y. Wang, B. Wang, Y. Yuan, K. Wang, Z. Mao, J. M. Rondinelli, and V. Gopalan, Observation of quasi-two-dimensional polar domains and ferroelastic switching in a metal, $Ca_3Ru_2O_7$, Nano Lett. **18**, 3088 (2018).

[25] W. Bao, Z. Q. Mao, Z. Qu, and J. W. Lynn, Spin valve effect and magnetoresistivity in single crystalline $Ca_3Ru_2O_7$, Phys. Rev. Lett. **100**, 247203 (2008).

[26] B. Bohnenbuck, I. Zegkinoglou, J. Strempfer, C. Schüßler-Langeheine, C. S. Nelson, P. Leininger, H.-H. Wu, E. Schierle, J. C. Lang, G. Srajer, S. I. Ikeda, Y. Yoshida, K. Iwata, S. Katano, N. Kikugawa, and B. Keimer, Magnetic structure and orbital state of $Ca_3Ru_2O_7$ investigated by resonant x-ray diffraction, Phys. Rev. B **77**, 224412 (2008).

[27] I. Marković, M. D. Watson, O. J. Clark, F. Mazzola, E. Abarca Morales, C. A. Hooley, H. Rosner, C. M. Polley, T. Balasubramanian, S. Mukherjee, N. Kikugawa, D. A. Sokolov, A. P. Mackenzie, and P. D. C. King, Electronically driven spin-reorientation transition of the correlated polar metal $Ca_3Ru_2O_7$, Proc. Natl. Acad. Sci. USA **117**, 15524 (2020).

[28] C. D. Dashwood, A. H. Walker, M. P. Kwasigroch, L. S. I. Veiga, Q. Faure, J. G. Vale, D. G. Porter, P. Manuel, D. D.

Khalyavin, F. Orlandi, C. V. Colin, O. Fabelo, F. Krüger, R. S. Perry, R. D. Johnson, A. G. Green, and D. F. McMorrow, Strain control of a bandwidth-driven spin reorientation in $Ca_3Ru_2O_7$, Nat. Commun. **14**, 6197 (2023).

[29] S. P. Ramkumar and E. A. Nowadnick, Octahedral rotations in Ruddlesden-Popper layered oxides under pressure from first principles, Phys. Rev. B **104**, 144105 (2021).

[30] T. Ishidate, S. Abe, H. Takahashi, and N. Môri, Phase diagram of $BaTiO_3$, Phys. Rev. Lett. **78**, 2397 (1997).

[31] E. Bousquet and P. Ghosez, First-principles study of barium titanate under hydrostatic pressure, Phys. Rev. B **74**, 180101(R) (2006).

[32] G. Clarke, D. Daisenberger, X. Luo, S. W. Cheong, N. C. Bristowe, and M. S. Senn, Pressure-dependent phase transitions in hybrid improper ferroelectric Ruddlesden-Popper oxides, Phys. Rev. B **109**, 094107 (2024).

[33] L. Leppert, S. E. Reyes-Lillo, and J. B. Neaton, Electric field- and strain-induced Rashba effect in hybrid halide perovskites, J. Phys. Chem. Lett. **7**, 3683 (2016).

[34] L. G. Davanse da Silveira, P. Barone, and S. Picozzi, Rashba-Dresselhaus spin-splitting in the bulk ferroelectric oxide $BiAlO_3$, Phys. Rev. B **93**, 245159 (2016).

[35] P. Z. Hanakata, A. S. Rodin, H. S. Park, D. K. Campbell, and A. H. Castro Neto, Strain-induced gauge and Rashba fields in ferroelectric Rashba lead chalcogenide PbX monolayers (X = S, Se, Te), Phys. Rev. B **97**, 235312 (2018).

[36] P. Noël, F. Trier, L. M. Vicente Arche, J. Bréhin, D. C. Vaz, V. Garcia, S. Fusil, A. Barthélémy, L. Vila, M. Bibes, and J.-P. Attané, Non-volatile electric control of spin–charge conversion in a $SrTiO_3$ Rashba system, Nature (London) **580**, 483 (2020).

[37] Y. Jin, J. Li, G. Wang, Q. Zhang, Z. Liu, and X. Mao, Giant tunable Rashba spin splitting in two-dimensional polar perovskites $TlSnX_3$ (X = Cl, Br, I), Phys. Chem. Chem. Phys. **24**, 17561 (2022).

[38] X. Wang, X. Li, H. Tian, H. Sang, J.-M. Liu, and Y. Yang, Anomalous Rashba effect driven by polar and nonpolar modes in the ferroelectric superlattice, J. Phys. Chem. C **126**, 20620 (2022).

[39] Q. Faure, C. D. Dashwood, C. V. Colin, R. D. Johnson, E. Ressouche, G. B. G. Stenning, J. Spratt, D. F. McMorrow, and R. S. Perry, Magnetic structure and field dependence of the cycloid phase mediating the spin reorientation transition in $Ca_3Ru_2O_7$, Phys. Rev. Res. **5**, 013040 (2023).

[40] K. Syassen, Ruby under pressure, High Press. Res. **28**, 75 (2008).

[41] G. M. Sheldrick, *SHELXT* – Integrated space-group and crystal-structure determination, Acta Crystallogr. Sect. A: Found Adv. **71**, 3 (2015).

[42] G. M. Sheldrick, Crystal structure refinement with SHELXL, Acta Crystallogr. Sect. C: Struct. Chem. **71**, 3 (2015).

[43] O. V. Dolomanov, L. J. Bourhis, R. J. Gildea, J. A. K. Howard, and H. Puschmann, OLEX2: a complete structure solution, refinement and analysis program, J. Appl. Crystallogr. **42**, 339 (2009).

[44] See Supplemental Material at http://link.aps.org/supplemental/10.1103/PhysRevB.111.205110 for high-pressure CIFs, refinement statistics, compressibility parameters, Birch-Murnaghan coefficients, and full computational details including the determination of the magnetic ground state and ambient band structure and the evolution of the band structure, magnetic moment, and Rashba spin splitting with pressure, which includes Refs. [23,25–27,45,47,48,51–60].

[45] M. J. Cliffe and A. L. Goodwin, PASCal: a principal axis strain calculator for thermal expansion and compressibility determination, J. Appl. Crystallogr. **45**, 1321 (2012).

[46] H. T. Stokes, D. M. Hatch, B. J. Campbell, and D. E. Tanner, ISODISPLACE: A web-based tool for exploring structural distortions, J. Appl. Crystallogr. **39**, 607 (2006).

[47] H. T. Stokes, D. M. Hatch, and B. J. Campbell, ISOTROPY Software Suite, iso.byu.edu, https://stokes.byu.edu/iso/isodistort.php

[48] S. Patel, U. Dey, N. P. Adhikari, and A. Taraphder, Electric field and strain-induced band-gap engineering and manipulation of the Rashba spin splitting in Janus van der Waals heterostructures, Phys. Rev. B **106**, 035125 (2022).

[49] https://www.archer2.ac.uk.

[50] G. Beckett, J. Beech-Brandt, K. Leach, Z. Payne, A. Simpson, L. Smith, A. Turner, and A. Whiting, ARCHER2 Service Description, Zenodo (2024), https://doi.org/10.5281/zenodo.14507040.

[51] G. Kresse and J. Furthmüller, Efficiency of *ab-initio* total energy calculations for metals and semiconductors using a plane-wave basis set, Comput. Mater. Sci. **6**, 15 (1996).

[52] G. Kresse and J. Furthmüller, Efficient iterative schemes for *ab initio* total-energy calculations using a plane-wave basis set, Phys. Rev. B **54**, 11169 (1996).

[53] J. P. Perdew, A. Ruzsinszky, G. I. Csonka, O. A. Vydrov, G. E. Scuseria, L. A. Constantin, X. Zhou, and K. Burke, Restoring the density-gradient expansion for exchange in solids and surfaces, Phys. Rev. Lett. **100**, 136406 (2008).

[54] P. E. Blöchl, Projector augmented-wave method, Phys. Rev. B **50**, 17953 (1994).

[55] G. Kresse and D. Joubert, From ultrasoft pseudopotentials to the projector augmented-wave method, Phys. Rev. B **59**, 1758 (1999).

[56] S. L. Dudarev, G. A. Botton, S. Y. Savrasov, C. J. Humphreys, and A. P. Sutton, Electron-energy-loss spectra and the structural stability of nickel oxide: An LSDA+U study, Phys. Rev. B **57**, 1505 (1998).

[57] K. Momma and F. Izumi, VESTA 3 for three-dimensional visualization of crystal, volumetric and morphology data, J. Appl. Crystallogr. **44**, 1272 (2011).

[58] D. Puggioni, M. Horio, J. Chang, and J. M. Rondinelli, Cooperative interactions govern the fermiology of the polar metal $Ca_3Ru_2O_7$, Phys. Rev. Res. **2**, 023141 (2020).

[59] M. Horio, Q. Wang, V. Granata, K. Kramer, Y. Sassa, S. Jöhr, D. Sutter, A. Bold, L. Das, Y. Xu *et al.*, Electronic reconstruction forming a C_2-symmetric Dirac semimetal in $Ca_3Ru_2O_7$, npj Quantum Mater. **6**, 29 (2021).

[60] A. M. León, J. W. González, and H. Rosner, $Ca_3Ru_2O_7$: Interplay among degrees of freedom and the role of the exchange correlation, Phys. Rev. Mater. **8**, 024411 (2024).